Flow Turbulence Combust (2013) 90:723–739
DOI 10.1007/s10494-011-9384-6

Simultaneous Measurements of Temperature and CO Concentration in Stagnation Stabilized Flames

Avinash Singh · Markus Mann · Thilo Kissel · Jan Brübach · Andreas Dreizler

Received: 2 May 2011 / Accepted: 30 November 2011 / Published online: 3 January 2012

Abstract An impinging jet burner was developed to investigate flame-wall interactions (FWI) using laser based diagnostics. CO concentrations were measured with two-photon laser-induced fluorescence (LIF) in combination with coherent anti-Stokes Raman spectroscopy (CARS) gas phase temperature measurements. Besides being the principal factor in chemical kinetics, temperature data is required to correct the CO LIF data for various factors like density variation, quenching and variation in the Boltzmann population. Phosphor thermometry was used to determine surface temperatures of the wall and to estimate the heat flux. In an parameter study Reynolds numbers and fuel equivalence ratio were varied.

Keywords Flame-wall interaction · CARS · CO LIF · Phosphor thermometry

1 Introduction

A majority of pollutants such as unburned hydrocarbons (UHC) and CO are produced in the near wall region in combustion systems. To enhance the efficiency of combustion engines, there is a general trend towards downsizing which, in turn, increases the surface to volume ratio. Moreover, in lean NO_x combustion engines, flames have been observed to be located much closer to the wall [1]. Considering these developments, the importance of near wall phenomena cannot be overstated. For a better understanding of flame structures close to walls, carefully designed experiments are needed which will also provide validation data for numerical simulations.

Carbon monoxide (CO) is an important species in combustion processes as an indicator of completeness of the process and as a pollutant. Therefore, the accurate

A. Singh · M. Mann · T. Kissel · J. Brübach · A. Dreizler (✉)
FG Reaktive Strömungen und Messtechnik, Center of Smart Interfaces,
Petersenstr. 32, 64287 Darmstadt, Germany
e-mail: dreizler@csi.tu-darmstadt.de

determination of its concentration in various flames is of crucial importance. A variety of techniques have been used for the CO determination like probe sampling [2], Raman scattering [3], tunable diode laser absorption spectroscopy [4, 5] and laser induced fluorescence (LIF) [6–8], with the laser induced fluorescence being the most commonly used.

Laser induced fluorescence is a well developed diagnostic technique because of its non-intrusive nature and excellent spatial as well as temporal resolution [9]. The energies of various energy states of the CO molecule predominantly lie in the VUV region [10], where a one-photon LIF cannot be used not only because of the inherent opacity of the air towards the VUV radiation but also due to the unavailability of lasers in that region. The use of a two-photon excitation circumvents both problems. Two-photon excitation of CO molecules to $B^1\Sigma^+$ [6–8] and $C^1\Sigma^+$ energy states have been reported [8].

In this work, the CO molecules were excited to the $B^1\Sigma^+$ state using two photons of 230.1 nm. The subsequent de-excitation to the $A^1\Pi$ state with the emission of the Ångström bands (λ = 451 to 725 nm) was detected.

The quantitative determination of species concentrations from LIF measurements is a challenging procedure due to numerous factors like collisional quenching, photoionization and broadband fluorescence interferences from other flame species [11].

The total collisional quenching rate of a molecule in an excited state can be calculated by multiplication of each quenching species concentration by the temperature-dependent species-specific quenching rate [12]. This approach requires the instantaneous knowledge of all of quenching-relevant species, which is not feasible in many experiments. Settersten et al. [12] measured the quenching coefficient values of major quenchers of CO(B) up to 1032 K and have suggested an extrapolation curve which can be used up to 2000 K.

In addition to the difficulty of determining of all quenching species concentrations in flames, the spectral overlap between linewidth of the excitation laser and absorption lines of the CO varies due to the temperature-dependent Boltzmann distribution of the electronic state. Thus, a calibration approach comparable to the one described in [13] was chosen for this study. A calibration polynomial was created based on reference LIF measurements in an electrically heated calibration gas jet and in a standard flat flame [14] at different temperatures.

Temperature is a crucial parameter in combustion, because it strongly affects all chemical reaction rates. In addition, an accurate determination of the temperature is a necessity in a quantitative LIF experiment. The absolute gas temperatures in the experiments were measured using the CARS technique which is described elsewhere [15]. CARS is expected to provide the most accurate, precise and non-invasive gas phase temperature, especially at flame temperatures [16]. Brübach et al. [17] measured gas phase temperatures as close as 30 μm to a convex surface.

In addition to the gas phase temperature, the wall surface temperature was also measured using thermographic phosphors (TP). TP are rare earth or transition metal doped ceramic materials which upon excitation by UV light undergo phosphorescence. The decay time and spectral characteristics of the phosphorescence vary as a function of temperature. Therefore, the temperature of phosphor-coated surfaces can be determined by measuring their decay lifetimes following laser excitation [15, 18].

Flame-wall interaction is a complex phenomenon and in general, a flame is quenched by the wall in a region in the close vicinity of the wall due to heat losses and fuel depletion [19]. In addition, the wall also limits the flame wrinkling and affects the turbulent flame as it influences the turbulence acting on the flame when the flame enters the near-wall region.

Brübach et al. employed phosphor and CARS thermometry simultaneously to determine surface-normal temperature gradients in impinging air jets [20], in flames [15] and within a technical combustor [17]. Salem et al. [21] determined heat flux with thermographic phosphors in combination with OH-LIF-thermometry in stagnation stabilized flames. In addition, Fuyuto et al. [22] measured OH, CO and CH_2O and temperature using of several LIF approaches and thermographic phosphor thermometry in a quenched boundary layer at a wall placed normal to a flat flame burner.

The present study reports on the simultaneous measurement of CO LIF, CARS gas phase thermometry and surface wall temperature determined by TP in an impinging jet burner. The gas phase temperature was used for correction of the CO LIF signal, whereas the surface wall temperatures of both sides of a wall gave us the heat flux through the wall. Along the centerline of the burner, the flame can be considered to be one-dimensional [23]. Calculations of a 1-D flame stagnated on a perpendicular wall were performed for comparison with the experimental values. The simulations were performed using Cantera [24] and GRI Mech 3.0 [25].

2 Experimental

2.1 Burner setup

The burner consisted of a nozzle of 30 mm in diameter positioned normal to a rotationally symmetric impingement disc, where the flame was stagnation-stabilized. The nozzle was surrounded by a 60 mm nitrogen coflow preventing the intrusion of ambient air into the flame (Fig. 1). The disc was made from stainless steel and quartz which were water-cooled and mounted on a linear stage with which the distance from the nozzle exit could be adjusted up to 3 nozzle diameters. To ensure homogeneous flow exiting the nozzle, a Morel nozzle design was applied. The interior of exit nozzle walls had a slight chamfer to prevent a recirculation of the fluid flow. The premixed methane flame was stable between Reynolds number $2000 < Re < 5000$, and there is a provision to further increase the jet turbulence by the use of an additional turbulence generator inside the nozzle.

The equivalence ratio Φ of the premixed methane air flow for the present experiment was varied between $0.83 < \Phi < 1.2$. The impingement disc had a slight convex curvature ($R = 300$ mm) to allow good optical access for focused laser beams in the near wall region. The wall mounting was insulated from the hot exhaust gases using heat shields and a suction. During the experiments, the temperature of the mount assembly remained less than 30 °C, so that thermal expansion of the mount was neglected. The final alignment was done before each experiment only after a certain warm up period.

The flow rates and mixture composition was controlled by thermal mass flow controllers (Bronkhorst). The accuracy of the used flow meters was better than 98%.

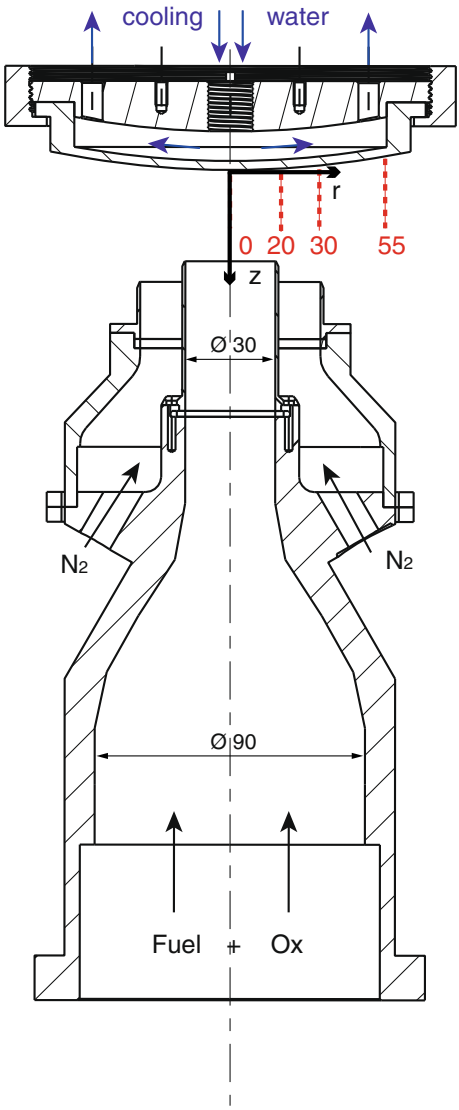

Fig. 1 Sketch of the FWI impinging jet burner. *Dashed lines* indicate measurement locations. z is set to zero at the wall surface for any radial position. All quantities are given in mm

2.2 CARS thermometry

Temperature measurements of the gas phase were performed using N_2 ro-vibrational CARS. This broadband method allows single pulse thermometry without tuning the Stokes laser through the N_2 spectrum. A frequency doubled 10 Hz Nd:YAG (Newport Quanta Ray PIV 400) laser was split into two beams, one part formed the pump and the probe beam, the other pumps a modeless dye laser generating the Stokes beam. With the pump and probe wavelengths of $\lambda_1 = \lambda_3 = 532$ nm and the Stokes wavelength centered around $\lambda_2 \approx 607$ nm, the difference frequency $\omega_1 - \omega_2$ approaches ω_v, the separation between two vibrational energy levels of N_2.

A more detailed description of the fundamentals of CARS can be found in [16] and [26].

The BOXCARS phase matching was achieved using a pair of 300 mm focus and parallelization lenses [27]. Laser pulse energies were adjusted using a combination of half-wave plate and polarizer cube for each beam. The size of the CARS probe volume, defined as the spatial overlap of the three laser beams, was 65 μm in diameter and 1.5 mm in beam direction which were determined by the FWHM values of a non-resonant CARS signal of a thin glass plate and a laser beam profiler.

The blue-shifted CARS signal was spectrally separated by two dichroic mirrors and a notch filter centered at 532 nm from the spatially overlapping pump beam. The CARS beam then was directed into a spectrometer (SPEX Industry, Spex 1707) with a focal length of 1 m and a 2400 lines/mm grating. The signal was collected by a CCD Camera (Princeton Instruments Pixis 400) with a chipsize of 1340 × 400 pixels. Because of the quadratic dependency of the CARS signal intensity on the fluid density, neutral density filters were used to prevent the CCD camera from saturation in lower temperature regions.

The measured spectra were background corrected and normalized by a mean non-resonant signal taken from 400 shots in pure methane immediately after each measurement. Theoretical spectra were fitted to the experimental data using the CARSFT algorithm [28] based on the least squares method. Typical precision of single-shot CARS temperature measurements was 2% at 2000 K.

2.3 CO LIF spectroscopy

The CO concentrations were measured by the use of two-photon LIF. The $B^1\Sigma^+(v'=0) \leftarrow\leftarrow X^1\Sigma^+(v''=0)$ Hopfield-Birge bands were excited by the absorption of two photons at 230.1 nm. The detection of the fluorescence emitted due to de-excitation from the $B^1\Sigma^+(v'=0) \rightarrow A^1\Pi(v''=1)$ transition was used for the experiments.

A frequency doubled Nd:YAG laser (Quanta-Ray GCR-4) pumped a dye laser (Sirah Precision Scan) operating with Pyridine 1 dye in ethanol, producing radiation at 690 nm which was frequency tripled using two BBO crystals. The laser wavelength was fine-tuned using the emission spectrum generated by a fuel rich flame of a flat flame burner [14]. The fluctuations in shot-to-shot laser energies were monitored by a photodiode which was positioned behind one of the mirrors. Laser pulse energies were in the range of 1.5 ± 0.1 mJ/pulse during the measurements. The UV laser light was then combined with the CARS beams and focused with a convex lens ($f = 300$ mm) into the probe volume. The emitted fluorescence light was collected by a combination of an achromatic lens ($f = 160$ mm) and a 100 mm $f/2$ lens (ZEISS Makro-Planar T* 100/2) and recorded by an intensified ICCD camera (Princeton Instruments PI-MAX II). To reduce the influence of crosstalk of the C_2 Swan bands [8], an interference filter with FWHM of 10 nm, centered at 484 nm was installed in front of the camera lens. The pixels of the CCD chip in beam direction were matched to the CARS probe volume and hardware-binned to reduce the pixel noise level. Since the B state of CO has a natural lifetime of 22 ns [12] as compared to the much longer lived C_2 [6], the camera gate was chosen to be 80 ns which also took care of jitter of the laser pulse.

The LIF signal intensity for a two-photon excitation following [7] can be written as

$$I_{LIF} = I_{OL}^2 \frac{A}{A + Q + P + RI_{OL}} \tag{1}$$

which is true, considering the nearly identical rotational constants of both X and B states of CO [29]. In this equation I_{OL} denotes the overlapping integral of the excitation radiation and the absorption cross section of the molecule, A denotes the fluorescence quantum yield, Q the quenching rate, P the predissociation rate and R the ionization rate. From equation 1, it is evident that the absorption rate is proportional to I_{OL}^2, however the LIF intensity I_{LIF}, will be in general proportional to I_{OL}^n where $1 < n < 2$, due to photoionization. By varying the laser energy, a calibration experiment was performed in the exhaust region of a flat flame and n was found to be 1.34 in our experimental setup. This factor was used for energy correction of the LIF signal.

Since the excitation laser has a fixed spectral width and temperature variation within a flame modifies the Boltzmann population distribution in CO molecules constantly, the spectral overlap between excitation laser and the CO absorption lines changes at different temperatures. Other processes like collisional quenching and predissociation are also affected by the temperature. A calibration polynomial comparable to [13] has been used, incorporating all the loss mechanisms for the CO LIF system. It was generated based on a heated jet of a CO-H_2-N_2 mixture up to 1000 K and up to 2200 K in a flat flame. The temperature range in between was interpolated. This calibration method reduces all the afore loss mechanisms to a temperature dependent third order polynomial.

For such simultaneous studies, the importance of a correct alignment of both laser systems cannot be overstated, as the temperature from the CARS measurement is used for LIF data correction. Therefore, an alignment routine was followed before each measurement series. After tuning the CARS to its best phase matching, the location of the CARS focus was ascertained by the non-resonant CARS signal of a thin glass plate. The laser beams were made to pass through a 100 μm pinhole. Afterwards the Rayleigh scattered light from the CARS beams was compared to the LIF in a flat flame and final adjustments were made.

In order to prevent a crosstalk between CARS and LIF, both systems were triggered with a time delay of 500 ns, which is below the typical timescales of turbulent transport scaling with at least a few 10 μs. The optical setup is shown in Fig. 2.

The image processing follows a procedure where an average background image was subtracted from the raw LIF images and then the signal from a probe volume matching to the CARS probe volume was integrated. Density correction using the CARS temperature and finally the calibration polynomial was used to account for the quenching losses and other factors described earlier. The LIF technique was validated by comparing it with measurements on a counter-flow diffusion burner as described in [30]. Typical SNR of single-shot CO measurements was in the order of 10–20 depending on the local CO concentration.

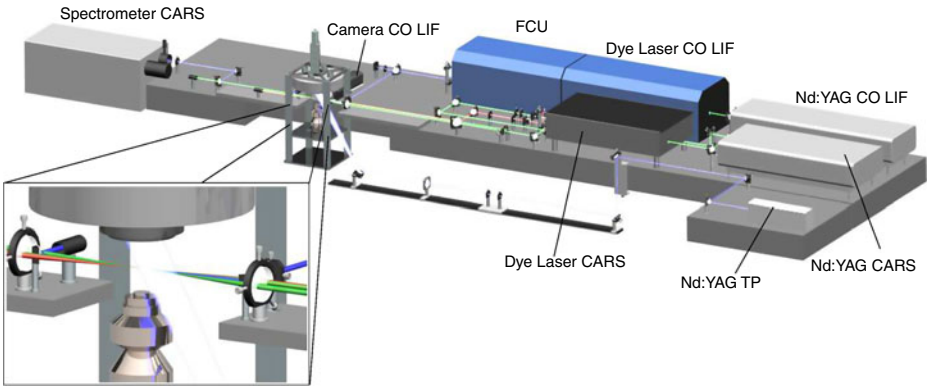

Fig. 2 Optical configuration of the CARS/CO LIF and TP experiments

2.4 Phosphor thermometry and heat flux estimations

For the measurement of surface temperatures of the wall, the impingement discs were coated with strips of Mg_4FGeO_6:Mn. The stainless steel plate was coated with a 2 mm × 60 mm strip on the flame-side, whereas in the case of the glass plate, both the flame-side as well as the water-cooled side had phosphor coatings for the estimation of the wall heat flux (Fig. 3).

The TP was excited with the third harmonic (355 nm) of a pulsed Nd:YAG laser (Quanta Ray INDI) at 10 Hz. Pulse energies were adjusted by the use of a glan polarizer in combination with a half-wave plate, so that the illuminance of the phosphor layer was maintained at 4 mJ/cm^2. The laser beam was expanded to the probe surface by 2 cylindrical lenses. The emitted phosphorescence was collected by a 85 mm lens (NIKKOR 85 mm f/1.4D) and recorded by a CMOS highspeed camera (LaVision HSS 6) operating at 20 kHz. The data was corrected as described in [31] and fitted by a mono-exponential waveform based on single pixel values and single shots according to [32].

The one-dimensional heat flux in the wall can be described by Fourier's Law of heat conduction

$$\dot{q} = \lambda_{hf} \frac{\mathrm{d}T}{\mathrm{d}z}, \tag{2}$$

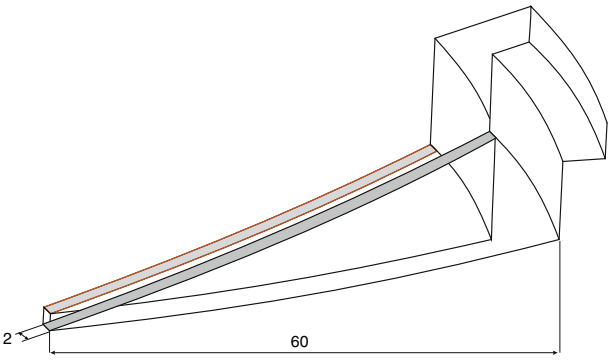

Fig. 3 Sketch of the dual layer phosphor coating of a segment of the impingement quartz wall. Dimensions are given in mm

where $\dot{q}$ is the heat flux, λ_{hf} is the conductivity of the medium and $\mathrm{d}T/\mathrm{d}z$ is the temperature gradient in the medium. Based on the measured temperatures, heat fluxes were calculated for the quartz wall and the gas phase next to the wall, whereas Cantera results were used to calculate the gas phase heat flux near the wall. For the quartz glass, the temperature gradient was calculated by dividing the difference in the temperatures of the two surfaces of the wall by the thickness of the wall. In the case of the gas phase heat flux near the wall, the temperature gradient was calculated by finding the difference between the flame-side surface temperature and the flame temperature closest to the wall.

For the heat flux estimated from the numerical simulations, the temperature gradient was evaluated from the temperatures of the final two grid points adjacent to the wall. The heat conductivity values are dependent on temperature as well as gas composition. λ_{hf} for the gas composition near the wall were calculated using the formula suggested by Wassiljewa [33] and Mason and Saxena [34]. The values of the thermodynamic quantities were taken from [35] while the gas composition near the wall was taken from the Cantera simulations.

2.5 1-D simulations

The 1-D stagnation flame simulations were carried out using the Cantera code [24]. The mechanism used was GRI 3.0 which included 325 elementary reactions and 53 species. The solution of this code calculates the momentum, energy, and species balances. The temperatures of the fuel mixture at the exit and at the stagnation wall were provided as boundary conditions and the wall was considered chemically inert. The gas temperature at the inflow to the computational domain was fixed at 300 K and the wall temperature was fixed at TP-measured temperatures. However the sensitivity of the flame to temperature changes of up to 50 K was negligible.

3 Results and Discussion

Time averaged, experimental temperature and CO concentration profiles for different radial positions of a lean laminar flame ($\Phi = 0.83$, $Re = 2000$) are shown in Fig. 4. This pre-experiment was carried out for demonstration purposes and the determination of the measurement positions. As there was a propensity for flashbacks for other equivalence ratios, Reynolds numbers for the subsequently investigated laminar case was raised from 2000 to 2500. All datapoints are an average of 400 single shots. CO LIF is corrected with the single-shot CARS temperatures of each measuring point. Both profiles at the inner radial positions ($r = 0$, 18 mm) show a similar behavior. The flame front, considered to be the zone of the highest temperature gradient, is located about 8 mm from the wall surface which matches with the maximum in CO concentration profile. In the region between the flame front and the wall, there is a slight increase in temperature up to 1960 K, while CO is getting oxidized. The influence of the boundary layer of the wall starts to be noticeable at a distance of 3 mm, where the temperature reduces sharply to the wall temperature while the CO concentration gradient further decreases. In the region close to the wall ($z < 0.15$ mm) there is a slight increase in the LIF signal

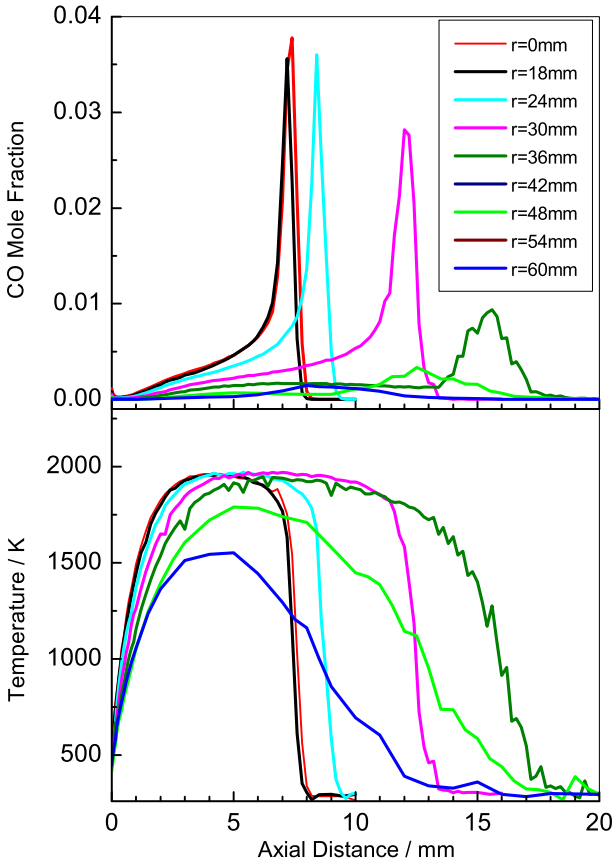

Fig. 4 Time averaged experimental temperature and CO profiles of a lean flame with $Re = 2000$ for different radial positions at the steel plate

due to an interaction of the excitation laser with the wall resulting in broadband fluorescence. With increasing radial positions, from $r = 18$ to 36 mm, the position of the flame front shifts away from the wall, with the flame at $r = 36$ mm having a steep temperature gradient at $z = 16$ mm. Moving away from the centerline, there is a decrease in the absolute values of both CO and temperature. At $r = 36$ mm, the CO concentration is about 25% of the value at $r = 0$ mm while the temperature reduces from 1960 K to 1940 K. The absolute values of both CO and temperature continues to decrease on further increasing radial positions but the apparent axial positions with the maximum temperature gradient shifts back towards the wall. However, the temperature gradient observed at $r > 36$ mm is much less compared to that closer to the center axis. This may imply that the thickness of the flame increases drastically as one approaches the edge of the stagnating wall. Noticing that the flame behaviour does not vary much at any radial position, further measurements were performed at $r = 0$, 20, 30 and 55 mm. In the following mean values from 200 single shots are presented, resulting in a signal to noise ratio (SNR) of about 50 for the single-shot CARS temperatures in the post flame zone and about 10–20 for the CO mole fractions.

3.1 Variation in fuel equivalence ratios

The mean value calculated from 200 single shots of the CO concentration and gas temperature as well as the mean surface temperature profiles are presented in Fig. 5 for different fuel equivalence ratios ($\Phi = 0.83$, 1.0 and 1.2) for a CH_4/air flame stabilized on a wall positioned at $z = 30$ mm from the nozzle. For the lean flame, there is a sudden increase in both CO and temperature at 7 mm from the wall. The CO profile attains a maximum at $z = 6.5$ mm and then shows a sharp decrease followed by a more gradual decrease as one approaches the wall. On the other hand, the temperature profile continues to rise more gently, reaching a maximum temperature of 1965 K at a distance of 4 mm from the wall before reducing sharply when moving towards the wall. In comparison to the lean flame, the stoichiometric flame displays the position of rise in the CO and temperature profiles at a distance of 11 mm from the wall indicating a higher burning velocity, which is also true for the fuel-rich flame front located at 10 mm wall-distance. The general CO concentration

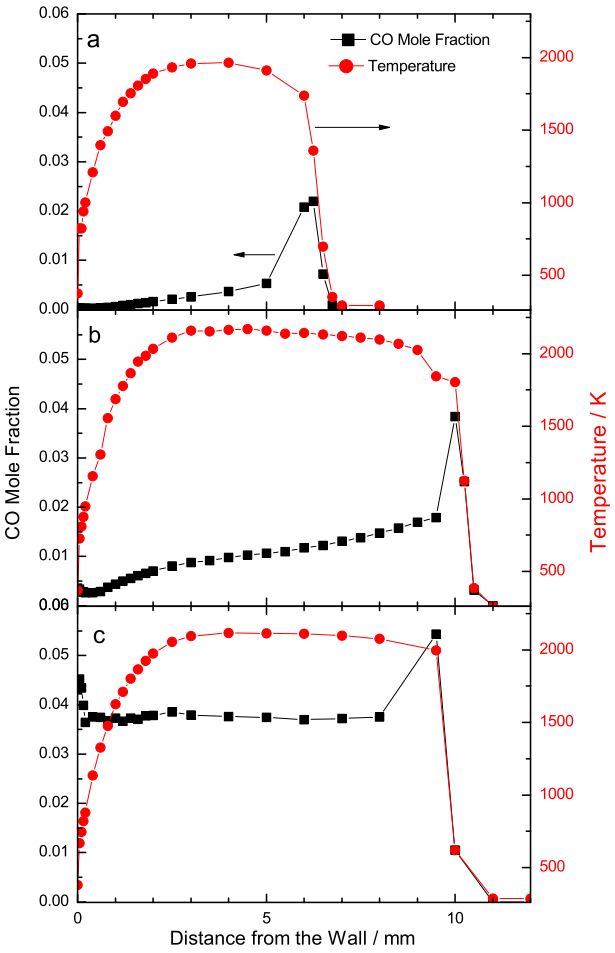

Fig. 5 Time averaged experimental axial temperature and CO profiles of a laminar flame with $Re = 2500$ at centerline position ($r = 0$ mm) at the steel plate for different fuel equivalence ratios: (**a**) $\Phi = 0.83$; (**b**) $\Phi = 1.0$ and (**c**) $\Phi = 1.2$

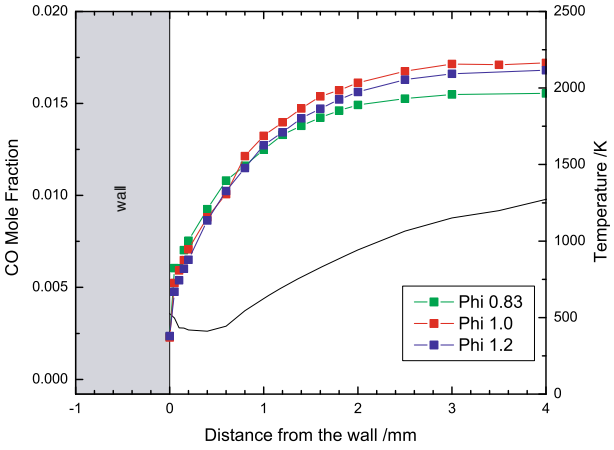

Fig. 6 Measured temperature profiles with corresponding surface temperatures (datapoints on the wall) for different equivalence ratios at $Re = 2500$ and CO concentration profile for $\Phi = 1$ (*solid black line*)

profiles of both lean and stoichiometric flames follow a similar trend, where the CO is consumed in the hot flame region. In contrast, in the fuel rich case the CO cannot be consumed in the post-flame zone, resulting in an almost constant mole fraction of 0.04.

Figure 6 shows the experimentally determined temperature profiles for the lean, stoichiometric and the rich flame ($Re = 2500$) close to the wall ($r < 4$ mm) and the CO profile for the stoichiometric flame. The point $r = 0$ denotes the surface temperature measured with phosphor thermometry. In the region close to the wall, there is a slight rise in the CO profile, where the LIF is influenced by reflections and wall interactions. The thickness of the thermal boundary layer for all equivalence ratios is about 2 mm.

3.2 Variation in Reynolds number

Figure 7a and b show the CO and the temperature profiles of a lean flame at Reynolds number 5000. Compared to Fig. 4, it is seen that the peak CO concentration decreases with an increase in Reynolds number and also the position of the flame front shifts much closer to the wall. The flame front for the centerline position is located at 3.75 mm from the wall as compared to 7.6 mm for a flame with $Re = 2000$. The maximum temperature at the centerline is slightly reduced in the case of the flame with higher Reynolds number (from 1965 K to 1940 K).

3.3 Variation in wall material

The experiments were also carried out with a wall made of quartz glass. The quartz wall being transparent, it was possible to measure the wall temperatures of both sides of the wall with the same experimental setup. The CO and the temperature profiles at different radial positions measured with a lean flame stagnating on a quartz wall are shown in Fig. 7c and d. As compared to similar measurements with the steel wall (Fig. 5a), there is no difference in the position of the flame front or the absolute peak values of CO and temperature.

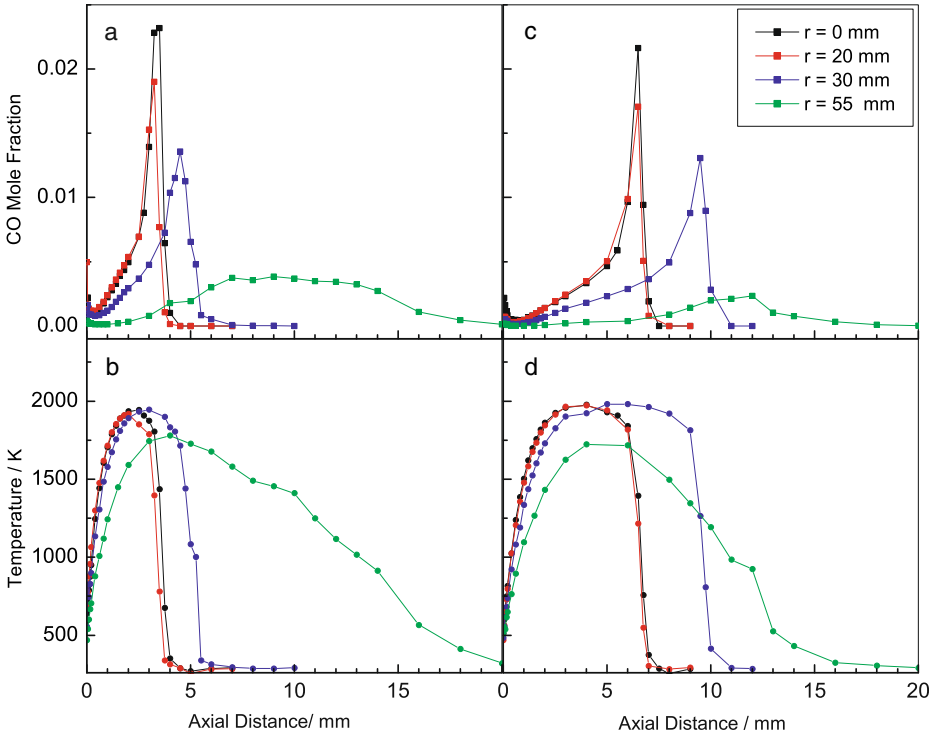

Fig. 7 Time averaged experimental axial temperature and CO profiles of a lean flame with $Re = 5000$ steel plate (*left*) and $Re = 2500$ for the quartz plate (*right*) for different radial positions

3.4 Comparison of experiment and simulation results

Figure 8 shows the comparison between the experimental and simulated values for a lean flame at a nozzle-wall distance of 30 mm for the centerline profile ($r = 0$). Simulations were carried out as a cross check for the measured data. It was not the

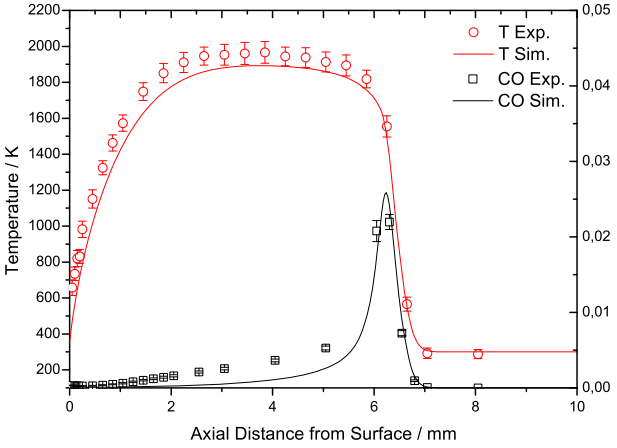

Fig. 8 Measured axial temperature and CO profiles and corresponding precision of a lean flame with $Re = 2500$ at $r = 0$ in comparison to the results obtained by Cantera simulation

intention of this paper to improve numerical simulations. Since the numerical code does not handle turbulent flows, simulations were only carried out for the laminar cases at $Re = 2500$. There is a good agreement in the temperature and CO profiles though there is a slight difference in the CO concentrations in the hot post-flame zone indicating the temperature-only based calibration polynomial overestimates the CO concentrations for the lean case. Since the exact localisation of the flame front position was not the aim of the present study, the measurements in the flame front region were not highly resolved resulting in the thickening of the experimental CO profiles at the flame front as compared to the Cantera results. However, Fig. 8 shows that the general shape of the experimental profiles agree well with the simulation results.

3.5 Heat flux measurements

The average of ten single-shot temperatures measured by TP of both sides of a quartz wall is shown in Fig. 9. The red and the blue lines correspond to the temperature profiles of the flame-side and water-cooled-side of the quartz wall. The flame-side surface was found to be hottest at the radial position $r = 0$ mm. The decreasing temperatures with increasing radial position are caused by the thickening of the boundary layer and thereby increasing distance between the hot gas region and the wall. Because of the low heat conductivity of quartz glass, the flame-side temperature varies over a range of 80 K with radial positions. Therefore the heat flux into the wall strongly depends on the radial position.

With a maximum temperature difference of 25 K, the water-cooled-side wall temperature profile (blue curve) is more homogeneous. The slight increase in the temperature of the water-cooled surface with increasing radial distance reflects the design of the cooling system, where the inlet is at the axis of symmetry and the centers of the 8 outlets are at a radial position of 46 mm. Temperature fluctuations at the water-cooled side were caused by gas bubbles produced on the

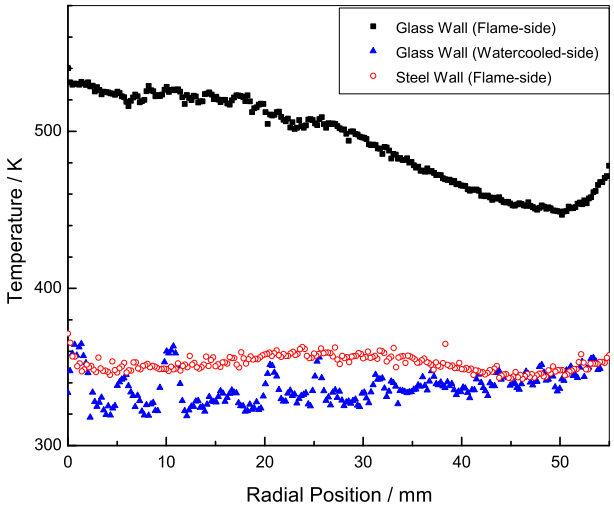

Fig. 9 Time averaged temperature profiles of both sides of the glass wall and the flame-side surface of the steel wall determined with phosphor thermometry

rough surface of the phosphor coating. Therefore the heat flux estimations were based on the temperature curve fits.

The 12 times higher thermal conductivity of stainless steel causes much lower temperatures on the flame-side surface (blue curve), which is in the same order as the temperature profile of the water-cooled quartz glass wall. The wavy structures observed in these profiles have been observed earlier in [36].

The heat flux of the quartz wall was calculated from these measurements and Fig. 10 shows the heat fluxes at different radial positions. For all three cases, the heat flux is maximum at the centerline and decreases with increasing radial distances. The lowest peak heat flux value of 86.8 kW/m^2 is measured for the lean flame while for the stoichiometric flame the value is 105.7 kW/m^2.

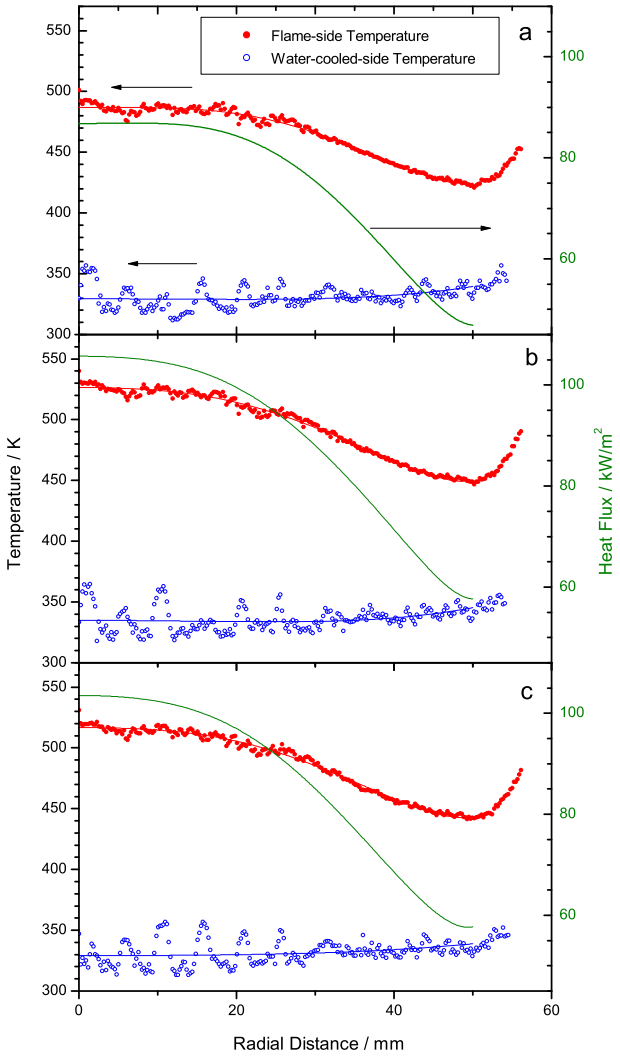

Fig. 10 Plots of the wall surface temperatures as a function of radial distance: (**a**) lean, (**b**) stoichiometric and (**c**) fuel rich flame (*red*: Flame side temperature, *blue*: water-cooled side). *Circles* denote measured data while *solid lines* represent the polynomial fits. Heat fluxes (*green lines*) were calculated based on the fitted temperature curves

The gas phase heat flux at the centerline using Cantera data was calculated using the last two grid points. Since the calculations do not take into account any radiative heat loss, the calculated results is likely to be underpredicted. The heat flux for a laminar flame, $Re = 2500$, at the centerline for three fuel equivalence ratios, $\Phi = 0.83$, 1.0 and 1.2 were found to be 70.7, 88.6 and 96.5 kW/m^2 while the corresponding values from the experimental data are 69.8, 83.9 and 103.3 kW/m^2.

4 Conclusion

In this study wall-normal CO concentration, gas phase temperature were measured simultaneously as well as wall surface temperatures on an impinging jet burner with high spatial resolution using laser based techniques. The results shown were based on single-shot diagnostics, allowing an instantaneous correction of LIF data, permitting the opportunity of measuring instationary and turbulent flames in further experiments. It was found that close to the wall coherent signals from CARS were not affected by the wall unlike in the case of LIF. Gas phase temperatures were measured as close as 35 μm from the wall while the CO LIF in distances less than 200 μm showed interferences from the wall and radiation interaction. No significant differences in the CO and temperature profiles were observed for the steel and glass walls. To the authors knowledge, it is the first time that simultaneous measurements of three scalars based on CARS, Two-Photon LIF and phosphor thermometry were carried out simultaneously. The experimental results of the centerline temperature and CO profiles match very well with the simulated 1-D simulations using detailed chemistry. For better understanding of the flame-wall interaction, it is necessary to carry out further studies extending the investigated parameters, such as turbulence intensity as well as wall properties. An extension to time resolved measurement techniques would allow an investigation of transient flame-wall interaction and the comparison of the measurements with numerical and theoretical results as reported in [37] and [38].

Acknowledgements The authors gratefully acknowledge the financial support of the DFG (Deutsche Forschungsgemeinschaft), EXC 259 (Center of Smart Interfaces) and GRK 1344.

References

1. Zhang, Y., Bray, K.N.C., Rogg, B.: Temporally and spatially resolved investigation of flame propagation and extinction in the vicinity of walls. Combust. Sci. Technol. **113**(1), 255–271 (1996)
2. Schoenung, M., Hanson, R.K.: CO and temperature measurements in a flat flame by laser absorption spectroscopy and probe techniques. Combust. Sci. Technol. **24**(5), 227–237 (1980)
3. Nooren, P.A., Versluis, M., van der Meer, T.H., Barlow, R.S., Frank, J.H.: Raman-Rayleigh-LIF measurements of temperature and species concentrations in the Delft piloted turbulent jet diffusion flame. Appl. Phys. B **71**, 95–111 (2000). doi:10.1007/s003400000278
4. Wang, J., Maiorov, M., Baer, D.S., Garbuzov, D.Z., Connolly, J.C., Hanson, R.K.: In situ combustion measurements of CO with diode-laser absorption near 2.3 μm. Appl. Opt. **39**(30), 5579–5589 (2000)
5. Chao, X., Jeffries, J.B., Hanson, R.K.: Absorption sensor for CO in combustion gases using 2.3 μm tunable diode lasers. Meas. Sci. Technol. **20**(11), 115201 (2009)
6. Aldén, M., Wallin, S., Wendt, W.: Applications of two-photon absorption for detection of CO in combustion gases. Appl. Phys. B **33**, 205–208 (1984)

7. Seitzman, J.M., Haumann, J., Hanson, Ronald K.: Quantitative two-photon LIF imaging of carbon monoxide in combustion gases. Appl. Opt. **26**, 2892–2899 (1987)
8. Linow, S., Dreizler, A., Janicka, J., Hassel, E.P.: Comparison of two-photon excitation schemes for CO detection in flames. Appl. Phys. B **71**, 689–696 (2000)
9. Rensberger, K.J., Jeffries, J.B., Copeland, R.A., Kohse-Höinghaus, K., Wise, M.L., Crosley, D.R.: Laser-induced fluorescence determination of temperatures in low pressure flames. Appl. Opt. **28**(17), 3556–3566 (1989)
10. Huber, K.P., Herzberg, G.: Molecular Spectra and Molecular Structure IV. Constants of Diatomic Molecules. Van Nostrand, New York (1979)
11. Kulatilaka, W.D., Patterson, B.D., Frank, J.H., Settersten, T.B.: Comparison of nanosecond and picosecond excitation for interference-free two-photon laser-induced fluorescence detection of atomic hydrogen in flames. Appl. Opt. **47**(26), 4672–4683 (2008)
12. Settersten, T.B., Dreizler, A., Farrow, R.L.: Temperature- and species-dependent quenching of CO B probed by two-photon laser-induced fluorescence using a picosecond laser. J. Chem. Phys. **117**(7), 3173–3179 (2002)
13. Barlow, R.S., Frank, J.H., Fiechtner, G.J.: Comparison of CO Measurements by Raman Scattering and Two-Photon LIF in Laminar and Turbulent Methane Flames. Spring Meeting of the Western States Section/The Combustion Institute (1998)
14. Gregor, M.A., Dreizler, A.: A quasi-adiabatic laminar flat flame burner for high temperature calibration. Meas. Sci. Technol. **20**, 065402 (2009)
15. Brübach, J., van Veen, E., Dreizler, A.: Combined phosphor and CARS thermometry at the wall-gas interface of impinging flame and jet systems. Exp. Fluids **44**, 897–904 (2008)
16. Eckbreth, A.C.: Laser Diagnostics for Combustion Temperature and Species. CRC, 2nd edn. (1996)
17. Brübach, J., Hage, M., Janicka, J., Dreizler, A.: Simultaneous phosphor and CARS thermometry at the wall-gas interface within a combustor. Proc. Combust. Inst. **32**(1), 855–861 (2009)
18. Brübach, J., Dreizler, A., Janicka, J.: Gas compositional and pressure effects on thermographic phosphor thermometry. Meas. Sci. Technol. **18**(3), 764–770 (2007)
19. Bruneaux, G., Poinsot, T., Ferziger, J.H.: Premixed flame/wall interaction in a turbulent channel flow: budget for the flame surface density evolution equation and modelling. J. Fluid Mech. **349**, 191–219 (1997)
20. Brübach, J., Zetterberg, J., Omrane, A., Li, Z.S., Alden, M., Dreizler, A.: Determination of surface normal temperature gradients using thermographic phosphors and filtered Rayleigh scattering. Appl. Phys. B **84**, 537–541 (2006)
21. Salem, M., Staude, S., Bergmann, U., Atakan, B.: Heat flux measurements in stagnation point methane/air flames with thermographic phosphors. Exp. Fluids **49**, 797–807 (2010)
22. Fuyuto, T., Kronemayer, H., Lewerich, B., Brübach, Jan., Fujikawa, T., Akihama, K., Dreier, T., Schulz, C.: Temperature and species measurement in a quenching boundary layer on a flat-flame burner. Exp. Fluids **49**, 783–795 (2010)
23. Egolfopoulos, F.N., Zhang, H., Zhang, Z.: Wall effects on the propagation and extinction of steady, strained, laminar premixed flames. Combust. Flame **109**(1–2), 237–252 (1997)
24. Goodwin, D.G.: An Open-Source, Extensible Software Suite for CVD Process Simulation (2003)
25. Gri-mech website. http://www.me.berkeley.edu/grimech (2006)
26. Stricker, W., Meier, W.: The use of CARS for temperature measurements in practical flames. Trends in Appl. Spectrosc. **1**, 231–260 (1993)
27. Eckbreth, A.C.: BOXCARS: Crossed-beam phase-matched CARS generation in gases. Appl. Phys. Lett. **32** (7), 421–423 (1978)
28. Clark, G., Farrow, R.L.: CARSFT Code. Sandia National Laboratory, Livermore, CA (1990)
29. Tobias, I., Fallon, R.J., Vanderslice, J.T.: Potential Energy Curves for CO*. J. Chem. Phys. **33**(6), 1683–1640 (1960)
30. Tsuji, H., Yamaoka, I.: The counterflow diffusion flame in the forward stagnation region of a porous cylinder. Symp. (Int.) on Comb. **11**(1), 979–984 (1967)
31. Kissel, T., Baum, E., Dreizler, A., Brübach, J.: Two-dimensional thermographic phosphor thermometry using a CMOS high speed camera system. Appl. Phys. B **96**, 731–734 (2009). doi:10.1007/s00340-009-3626-5
32. Brübach, J., Janicka, J., Dreizler, A.: An algorithm for the characterisation of multi-exponential decay curves. Opt. Laser Eng. **47**(1), 75–79 (2009)
33. Reid, R.C., Prausnitz, J.M., Poling, B.E.: The Properties of Gases and Liquids. McGraw Hill (1987)

34. Mason, E.A., Saxena, S.C.: Approximate formula for the thermal conductivity of gas mixtures. Phys. Fluid **1**, 361–369 (1958)
35. VDI - Gesellschaft Verfahrenstechnik und Chemie-ingenieurwesen (eds.): VDI-Wärmeatlas. Springer (2002)
36. Hofmann, H.M.: Wärmeübergang beim pulsierenden Prallstrahl. PhD thesis, Universität Fridericiana Karlsruhe (2005)
37. Popp, P., Baum, M.: Analysis of wall heat fluxes, reaction mechanisms, and unburnt hydrocarbons during the head-on quenching of a laminar methane flame. Combust. Flame **108**(3), 327–348 (1997)
38. Wichman, I.S., Bruneaux, G.: Head-on quenching of a premixed flame by a cold wall. Combust. Flame **103**(4), 296–310 (1995)